ANALYSIS OF A NOVEL MEMS GYROSCOPE ACTUATED BY PARAMETRIC RESONANCE

Nicholas J. Miller
Department of Mechanical Engineering
Michigan State University
East Lansing, Michigan 48824, USA
mille820@msu.edu

Steven W. Shaw
Department of Mechanical Engineering
Michigan State University
East Lansing, Michigan 48824, USA
shawsw@msu.edu

Laura A. Oropeza-Ramos
Department of Mechanical Engineering
University of California, Santa Barbara
Santa Barbara, California 93106, USA
loropeza@engineering.ucsb.edu

Kimberly L. Turner
Department of Mechanical Engineering
University of California, Santa Barbara
Santa Barbara, California 93106, USA
turner@engineering.ucsb.edu

Abstract

An analysis of a nonlinear MEMs gyroscope operating under parametric resonance is presented. Drive frequency and rotation rate responses are presented, and it is shown that this gyroscope is robust under frequency mistuning. Solution structures are developed from a simplified system and limiting behavior is considered for the complete system. Numerical examples are presented in support of the analytical results. The findings support preliminary experimental results.

1 Introduction

Vibrating MEMs Gyroscopes commonly function on the coupling of two linear resonant modes via the Coriolis force. Such devices employ a proof mass constrained to move in a plane with two resonant modes which are nominally orthogonal. The two modes are ideally coupled only by the rotation of the gyro about the plane's normal vector. High rate sensitivity for such devices requires high resonance quality and matched modal frequencies for the two orthogonal modes (Yazdi *et al.*, 1998).

These design requirements, orthogonality and frequency matching, are not generally robust under parameter uncertainty. Frequency missalignment causes substantial decrease in rate sensitivity, and model missalignment causes erroneous rate measurement, genereally referred to as quadrature error (Shkel *et al.*, 1999). Accordingly, there is sufficient motivation to produce a gyroscope design that is robust to fabrication tolerances. There has been a great deal of research into gyroscope design, and a myriad of gyroscopic structures have been produced including beam, tuning fork, ring, and gymbol designs (Yazdi *et al.*, 1998; Esmaeili *et al.*, 2007; Zaman *et al.*, 2004; Ayazi and Najafi, 2001). An alternate, but complementary, approach to dealing with parameter uncertainty is to accept the uncertainty and use of feedback control to counter its effects. Feedback compensation for fabrication tolerance has been extensively studied, and several successful strategies have been developed including frequency tuning and adaptive mode correction techniques, among others (Park and Horowitz, 2003; Leland, 2003; Wang *et al.*, 2006; Gallacher *et al.*, 2005).

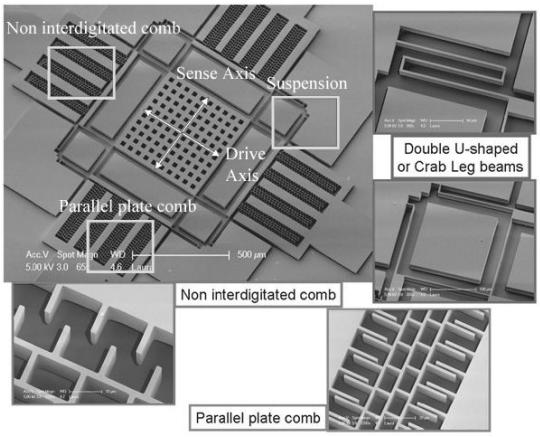

Figure 1. Micrograph image of the gyroscope. This device was fabricated on an SOI wafer with a $20\mu m$ silicon layer over a $5\mu m$ insulator using a single mask process

Some of the more novel approaches include Acar and Shkel's nonresonant 4 DOF gyroscope (Acar and Shkel, 2003). In this device, a 4 degree of freedom vibrating structure is designed such that the frequency

responses for the drive and sense axis resonators are flat, yet large, around the operating frequency. This flat portion of the frequency response is away from the resonant frequencies, and thus robust to small variation in natural frequencies and damping ratios. This design attempts to eliminate mode matching requirements and minimize instability and drift.

Another novel approach is the parametric resonance based gyroscope presented by Oropeza-Ramos *et al.* (Oropeza-Ramos, 2007; Oropeza-Ramos and Turner, 2005). This device utilizes the broad and flat frequency response of a parametric resonance to produce a gyroscope that is robust to frequency mistuning and damping effects. This gyroscope has been successfully demonstrated in experiments by Oropeza-Ramos *et al.* This gyroscope is the only MEMs gyro that utilizes nonlinear vibration principles known to the authors.

While parametric resonance in MEMs has been previously studied (Turner *et al.*, 1998; Rhoads *et al.*, 2005; Turner, 1999), this gyroscope features coupling of two duffing type resonators with parametric excitation, and the dynamics of this are not fully understood. In this letter, we analyze the response structure of this gyroscope and show that the parametric resonance provides insensitivity to the frequency matching and quality factor requirements of more conventional devices. Accordingly, in section 2 we present the model for the device and transform it via averaging into a form amenable to analysis. In section 3, we consider the frequency response of the system, and in section 4 we consider the rotation rate response. Conclusions are presented in section 5.

2 Model

A micrograph image of the gyroscope is shown in figure 1 (Oropeza-Ramos, 2007). This device consists of a perforated proof mass constrained to move in the plane by a suspension of microbeams. It is forced along one axis, the so called drive axis, by a set of non-interdigitated comb drives, and its motion along the other axis, the sensing axis, is detected by a set of parallel plate capacitors.

In previous work, (Oropeza-Ramos *et al.*, 2007), it has been shown that this system can be modeled by the set of ordinary differential equations

$$\begin{aligned} &m\ddot{x} + c\dot{x} + [k_{11} + r_1 V_a^2(1+\cos(2\omega t))]x + \\ &\quad [k_{31} + r_3 V_a^2(1+\cos(2\omega t))]x^3 - 2\Omega\dot{y} = 0, \quad (1)\\ &m\ddot{y} + c\dot{y} + k_{12}y + k_{32}y^3 + 2\Omega\dot{x} = 0. \end{aligned}$$

Here, x is the displacement along the drive axis, y is the displancement along the sense axis, m is the sensor mass, c is the viscous dissipation constant, k_{11} is the drive axis linear stiffness, r_1 is the linear electrostatic forcing constant, k_{31} is the cubic stiffness coefficient, r_3 is the nonlinear electrostatic forcing constant, k_{12} is the sense axis linear stiffness, and k_{32} is the sense axis nonlinear stiffness coefficient. Ω is the rotation rate of the gyroscope about the axis normal to the plane of the gyroscope. In order to reduce the number of free parameters and facilitate analysis, we nondimensionalize equations (1). We also take this opportunity to introduce scaling arguments via the small parameter ϵ.

Table 1. Nondimensional parameter definitions for equations 2. Here L represents some characteristic length.

$q_d = \frac{x}{L}$	$q_s = \frac{y}{L}$
$\tau = t\sqrt{\frac{m}{k_{11}}}$	$\epsilon\zeta = \frac{c}{\sqrt{mk_{11}}}$
$\epsilon\lambda_1 = \frac{r_1 V_a^2}{k_{11}}$	$\epsilon\nu_3 = \frac{k_{31}L^2}{k_{11}}$
$\epsilon\lambda_3 = \frac{r_3 L^2 V_a^2}{k_{11}}$	$\epsilon\gamma = 2\Omega\sqrt{\frac{m}{k_{11}}}$
$\epsilon\delta = \frac{k_{12}}{k_{11}} - 1$	$\epsilon\xi = \frac{k_{32}L^2}{k_{11}}$

$$\begin{aligned} &q_d'' + 2\epsilon\zeta q_d' + [1 + \epsilon\lambda_1(1+\cos(2\omega\tau))]q_d + \\ &\quad [\epsilon\nu_3 + \epsilon\lambda_3(1+\cos(2\omega\tau))]q_d^3 - \epsilon\gamma q_s' = 0, \quad (2)\\ &q_s'' + 2\epsilon\zeta q_s' + (1+\epsilon\delta)q_s + \epsilon\xi q_s^3 + \epsilon\gamma q_d' = 0. \end{aligned}$$

The definitions of the nondimensional parameters are given in table 1. Applying the method of averaging to these equations produces a set of slowly time varying differential equations which govern the amplitudes and phases of the drive and sense axis resonators. To do this, we assume a near-resonance condition, $\omega = 1 + \epsilon\sigma$; this results in

$$\begin{aligned} a_1' =& \frac{\epsilon}{8}[4a_2\gamma C_{12} + a_1(-8\zeta + \\ &(2\lambda_1 + \lambda_3 a_1^2)\sin(2\psi_1))],\\ a_2' =& \frac{-\epsilon}{2}[a_1\gamma C_{12} + 2\zeta a_2],\\ \psi_1' =& \frac{\epsilon}{8a_1}[-4a_2\gamma S_{12} + a_1(4\lambda_1 - 8\sigma + \\ &3(\nu_3+\lambda_3)a_1^2 + 2(\lambda_1 + \lambda_3 a_1^2)\cos(2\psi_1))],\\ \psi_2' =& \frac{\epsilon}{8a_2}[-4a_1\gamma S_{12} + a_2(4\delta - 8\sigma + 3\xi a_2^2)],\\ C_{12} =& \cos(\psi_1 - \psi_2),\\ S_{12} =& \sin(\psi_1 - \psi_2). \end{aligned} \quad (3)$$

Here, a_1 is the amplitude of oscillation along the drive axis, and a_2 is the amplitude of oscillation along the sensing axis. ψ_1 and ψ_2 are the phases of oscillation for the two axes.

3 Frequency Response Analysis

Unfortunately, these equations do not admit closed form solutions for the fixed points, and so we are forced to take a less direct approach. Since we cannot solve the general system, we solve a simplified case, and then use those solutions to develop some understanding of

the general case. Accordingly, we consider the slightly simplified case where the sense axis is linear, and there is no damping. Hence, $\zeta = 0$ and $\xi = 0$.

Equations (3), with the aforementioned simplifications, yield the amplitude solutions

$$a_1 = 0, \sqrt{\frac{\frac{4\gamma^2}{\delta - 2\sigma} + 8\sigma - 6\lambda_1}{3\nu_3 + 2\lambda_3}}, \sqrt{\frac{\frac{4\gamma^2}{\delta - 2\sigma} + 8\sigma - 2\lambda_1}{3\nu_3 - 2\lambda_3}}, \tag{4}$$

$$a_2 = a_1 \sqrt{\frac{\gamma^2}{(\delta - 2\sigma)^2}} \tag{5}$$

Though the details are omitted for brevity, equations (4) and (5) give a frequency response solution that has four branches departing from the zero solution at frequencies described by the detuning values

$$\sigma_{1,2} = \frac{1}{4}\left(\delta + \frac{3\lambda_1}{2} \pm \sqrt{4\gamma^2 + (\delta - \frac{3\lambda_1}{2})^2}\right)$$
$$\sigma_{3,4} = \frac{1}{4}\left(\delta + \frac{\lambda_1}{2} \pm \sqrt{4\gamma^2 + (\delta - \frac{\lambda_1}{2})^2}\right)$$

Again, the detuning values, σ, are related to the forcing frequency by $\omega = 1 + \epsilon\sigma$. This can be seen in figure 2, where the response for a gyroscope with a hardening drive axis, linear sense axis, and zero damping is shown. In this, and all other figures in this letter, heavy solid lines respresent stable fixed points, light dashed lines represent unstable fixed points. The parameters chosen for this plot represent a gyro with the dimensional parameters given in table 2. The direction in which these branches bend can exhibit hardening, softening, or mixed behavior, depending on mechanical and electrostatic nonlinearities. The mechanical nonlinearity is typically hardening, but the electrostatic nonlinearity can be either hardening or softening, depending on the alignment of the noninterdigitated combs, see figure 1. In this letter, we consider only hardening behavior since neither mixed nor softening behavior offer any additional benefit. The frequency response for a gyroscope with a hardening drive axis will conform to the structure of the response shown in figure 2. The solutions branching from $\sigma_{1,3}$ (those on the left) are separated from those branching from $\sigma_{2,4}$ (those on the right) by a vertical asymptote at $\sigma = \frac{\delta}{2}$, the location of the sensing axis resonance.

Considering the response structure shown in figure 2, we can make a qualitative argument explaining why this gyroscope is robust to frequency mistuning between drive and sense axis resonators. The drive axis response is approximately a parametric resonance frequency response structure, and the sensing axis response is approximately the product of the parametric resonance frequency response and the linear frequency response of the sensing resonator. Figure 3

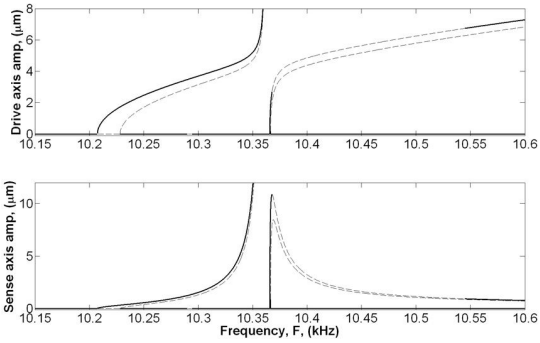

Figure 2. Frequency response for gyroscope with linear sense axis and zero damping, $\zeta = \xi = 0$, under rotation $\Omega = 160$Hz.

Table 2. Dimensional gyroscope parameters for example plots

$m = 1.4e-8\ kg$	$f_d = 10.244\ kHz$
$f_s = 10.361\ kHz$	$k_3 = 0.12\ \frac{\mu N}{\mu m^3}$
$r_1 = -3.9e-4\ \frac{\mu N}{\mu m V^2}$	$r_3 = -9.9e-6\ \frac{\mu N}{\mu m^3 V^2}$
$\epsilon = 0.001$	$L = 1\mu m$

shows, in the drive axis plot, the frequency response with a parametric resonance response superimposed. The response structure of the drive axis resembles that of parametric resonance, though it is split, so to speak, at natural frequency of the sensing axis resonator. This splitting occurs as a result of the coupling between the resonators. The effect of the coupling becomes dramatic when the response of the sensing resonator becomes large, as it does near resonance. Furthermore, the frequency response of the sensing axis closely resembles the product of a parametric resonance frequency response and a linear frequency response. The sense axis plot in figure 3 shows such a product superimposed on the sense axis frequency response. From these observations, we can argue that the response of sensing resonator will be large as long as its natural frequency lies in the frequency range of the drive axis's parametric resonance. This frequency range appears in figures 2 and 3, to persist for all frequencies greater than the drive axis natural frequency. This is because we have not included nonlinear damping in our model, for simplicity. The reader should bear in mind that these non-zero frequency response structures will terminate eventually due to nonlinear damping effects. However, the qualitative nature of these results do match that of the experimental results in the forementioned works. Currently, damping studies have not yet been performed experimentally, and so the verification of this simplifying assumption is left to future work.

Since parametric resonance offers a wide and flat resonance structure, small changes in the sensing axis's natural frequency will affect the amplitude of the re-

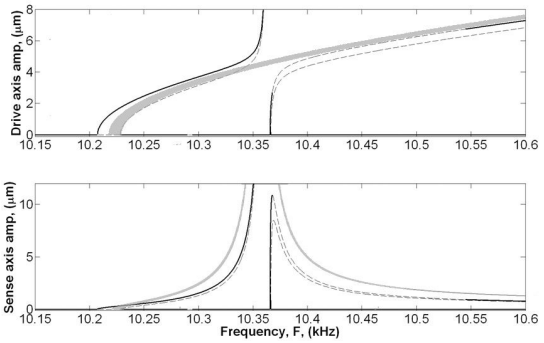

Figure 3. Gyroscope frequency response, as in figure 2, with parametric resonance response overlay (in light gray) on drive axis and linear system response to parametric resonance overlay (in light gray) on sense axis.

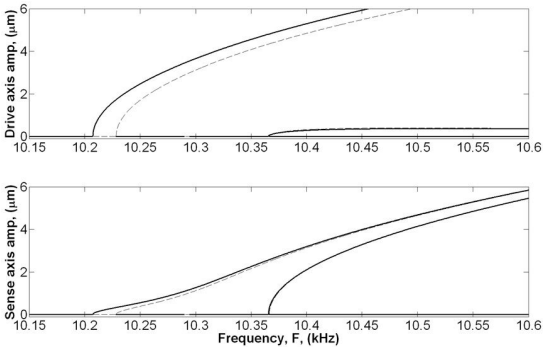

Figure 4. Frequency response for gyroscope with zero damping, $\zeta = 0$, under rotation rate $\Omega = 160$Hz.

sponse very little. Consequently, as long as the sense axis natural frequency lies in this range, the resulting sense response will also be relatively unaffected. This is a somewhat simplified view of things, but it certainly does illustrate why this gyroscope is robust under frequency mistuning between the drive and sense axis resonators.

In order to extend this analysis to the general system, consider the effects of nonlinearity on the sensing resonator. A hardening nonlinearity will bend the sensing resonator's frequency response to the right. This effect is amplitude dependant and so, we expect the branch that follows the vertical asymptote to bend. The low amplitude structure, however, should remain nearly the same. The branch points in particular should not be affected at all. Also, we expect to see these changes in the sensing resonator's response reflected in the drive resonator's response. Indeed, this is what happens. Figure 4 shows the frequency response for the gyroscope with the hardening nonlinearity included in the sensing resonator ($\xi \neq 0$).

Nonlinearity in the sensing resonator bends the frequency response structure so that both drive and sense axis resonator's have frequency responses similar to a single duffing equation under parametric resonance.

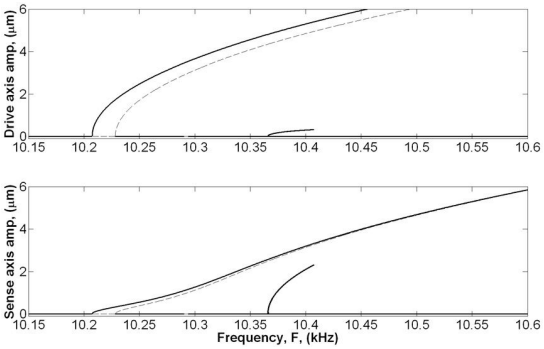

Figure 5. Frequency response for gyroscope with damping, $\zeta = 0.1$, under rotation rate $\Omega = 20.38$Hz.

The major difference here, however, is the existence of this second lower amplitude solution. Since dissipation in a duffing resonator under parametric excitation changes the frequency response only a small amount (Oropeza-Ramos and Turner, 2005), we expect that these response structures will not change much in the presence of damping. Figure 5 shows the same frequency response with small damping added. The higher amplitude branches are mostly unaffected, but the lower amplitude branch is nearly destroyed. For large damping values, this branch will be completely destroyed.

The focus of this analysis is on stable periodic solutions of the gyroscope equations of motion, equations (1), or equivalently, stable fixed points of the average equations, equations (3). Accordingly, we did not follow any branches of periodic solutions in the average equations. However, it turns out that the small window of instability that appears on the zero solution branch around 10.29 kHz is the result of a Hopf bifurcation. It is currently unclear if this feature is a cause of concern. The current experimental results have not reported any quasiperiodic or other nonperiodic behaviors.

4 Rate Response Analysis

The frequency response of this gyroscope, particularly with hardening sensing resonator, offers a large range of operating frequencies which provide large response amplitudes. Let us consider how these operating points change with rotation rate. For the simplified system, equations (4) and (5) provide the answer directly. Additionally, a qualitative understanding of the rate response structure can be obtained by considering limiting cases of the equations. These equation show that when

$$\frac{4\gamma^2}{\delta - 2\sigma} \gg 8\sigma - 6\lambda_1 \tag{6}$$

or

$$\frac{4\gamma^2}{\delta - 2\sigma} \gg 8\sigma - 2\lambda_1, \tag{7}$$

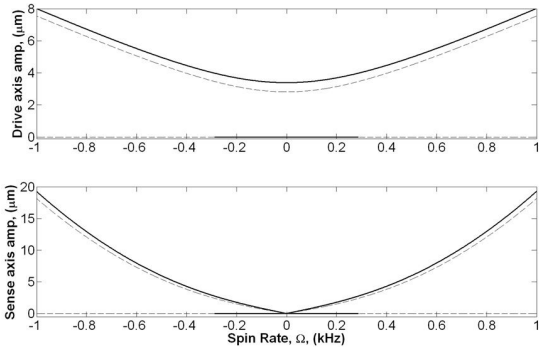

Figure 6. Rotation rate response for gyroscope with linear sense axis and zero damping, $\zeta = \xi = 0$. Drive frequency $F = 2\pi\omega = 10.2952$kHz

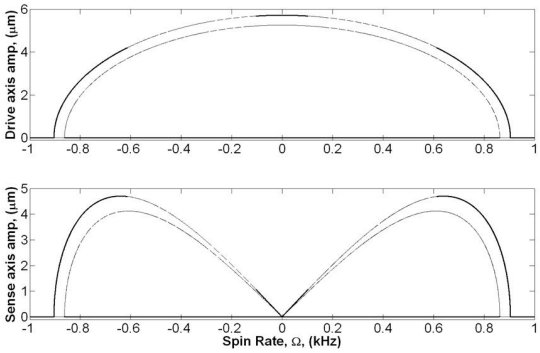

Figure 7. Rotation rate response for gyroscope with linear sense axis and zero damping, $\zeta = \xi = 0$. Drive frequency $F = 2\pi\omega = 10.4489$kHz

then

$$a_1 \propto \gamma, \qquad a_2 \propto \gamma^2. \tag{8}$$

Here, a_1 and a_2 represent the drive and sense axis solution branches that correspond with the appropriate relative magnitude statement, (6) or (7). Accordingly, figure 6 shows the amplitude solutions for the simplified system with respect to spin rate. In this figure, we see that, for large spin rate, the dive axis amplitude is nearly linear and the sense axis amplitude nearly quadratic. Similarly, when

$$\frac{4\gamma^2}{\delta - 2\sigma} \ll 8\sigma - 6\lambda_1 \tag{9}$$

or

$$\frac{4\gamma^2}{\delta - 2\sigma} \ll 8\sigma - 2\lambda_1, \tag{10}$$

then

$$\frac{\partial a_1}{\partial \gamma} \approx 0, \qquad a_2 \propto \gamma. \tag{11}$$

Thus, in figure 6, we see that, for small Ω, the drive axis amplitude is constant, and the sense axis is amplitude is linear. Figure 6 shows the rate response of the simplified gyroscope for a frequency below the natural frequency of the sense axis resonator. If we consider the rate response for a frequency above the sense axis's natural frequency, we find a rate response like the one shown in figure 7. In this case, the nonzero rate response exists in a finite range which depends on the frequency of operation, and it does not posses a stable solution over that entire range. Clearly, such a mode of operation is not amenable to rate sensing.

For the general system, we cannot produce equations that give the rate response explicitly as for the simplified system. However, for the system without damping ($\zeta = 0$), we can gain some insight into the rate response by considering limiting cases similar to the above. For the zero damping case, equations (3) yield two polynomials in a_1 and a_2 respectively, whose roots describe the fixed points of the averaged system. For the sake of brevity, the details are omitted, but suffice it to say that these polynomials are of the forms

$$\begin{aligned} a_1 P_{1,4}(a_1^2) &= 0, \\ a_2 P_{2,4}(a_2^2) &= 0. \end{aligned} \tag{12}$$

Here, $P_{1,4}$ and $P_{2,4}$ are the fourth order polynomials associated with a_1 and a_2 respectively. Equation (12) shows, naturally, that $a_1 = 0$ and a_2=0 are solutions. More interestingly is the result that for the limiting case of small, $O(\epsilon)$, amplitude and spin rate, the amplitudes depend linearly on spin. Thus,

$$a_1 \propto \gamma, \qquad a_2 \propto \gamma. \tag{13}$$

For the limiting case of large amplitude, $O(\epsilon^{-1})$, and larger spin rate, $O(\epsilon^{-2})$, the amplitudes depend on the square root of the spin rate. Hence,

$$a_1 \propto \sqrt{\gamma}, \qquad a_2 \propto \sqrt{\gamma}. \tag{14}$$

Accordingly, in figure 8, which corresponds to the same operating conditions as in figure 6, except here the sense axis stiffness is nonlinear, we find that for small spin rate, a_2 is linear with respect to spin. a_1 is not, however. This is because a_1 is not small. Also, for large spin rates, both amplitudes are large and vary with the square root of the spin rate.

Interestingly, If we examine the rate response for the same operating point as in figure 7, except now including the nonlinear sensing stiffness, we find a more complex structure with additional solution branches. This is shown in figure 9. Additional solution branches are to be expected. This can easily be seen by a comparison of

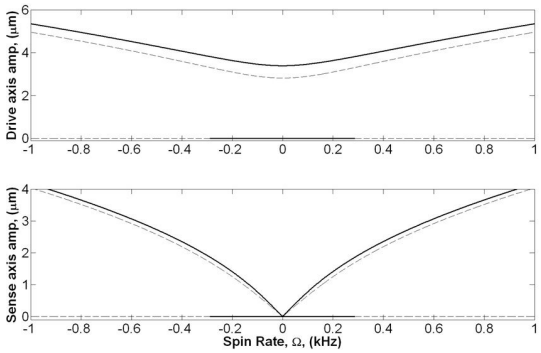

Figure 8. Rotation rate response for gyroscope with nonlinear sense axis and zero damping, $\zeta = 0$. Drive frequency $F = 2\pi\omega = 10.2952$kHz

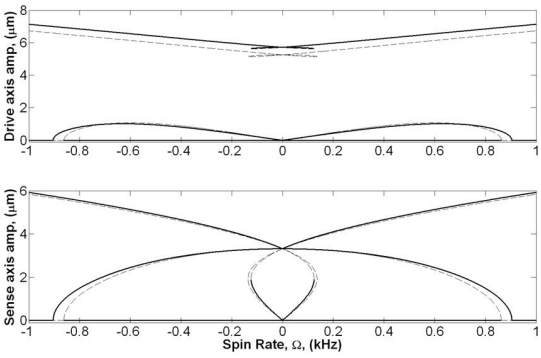

Figure 9. Rotation rate response for gyroscope with nonlinear sense axis and zero damping, $\xi = 0$. Drive frequency $F = 2\pi\omega = 10.4489$kHz

the frequency responses, at the appropriate frequency, for the cases of a linear and nonlinear sense axis: figures 2 and 4 respectively. The stability of the nonzero solutions has also changed from the linear case, showing that operating above the sense axis linear natural frequency is possible when the sense axis resonator is nonlinear.

5 Conclusions

In this letter, we present analysis of a nonlinear MEMs gyroscope which operates on parametric resonance in duffing type resonators. The coupling of two duffing resonators forced by parametric excitation produces a complex system which is not very amenable to direct formulations for the steady state solutions. Consequently, we approached this analysis by considering the simplified case of an undamped parametrically forced duffing resonator coupled to an undamped linear resonator. We then extended this solution to the complete case obtaining qualitative information and limiting behavior for the response structure. We also produced numerical solutions to support our findings. This work provides useful analysis for design and evaluation of this gyroscope design, though it still needs to be correlated in a systematic way to experimental results.

Acknowledgements

The authors would like to acknowledge Jeffrey F. Rhoads for his assistance. This material is based on work supported by the National Science Foundation under grant No. ECCS-0428916. Any opinions, findings, conclusions or recommendations expressed in this material are those of the authors and do not necessarily reflect the views of the National Science Foundation.

References

Acar, Cenk and Andrei M. Shkel (2003). Nonresonant micromachined gyroscopes with structural mode-decoupling. *IEEE Sensors Journal* **3**(4), 497–506.

Ayazi, Farrokh and Khalil Najafi (2001). A harpss polysilicon vibrating ring gyroscope. *Journal of Microelectromechanical Systems* **10**(2), 169–179.

Esmaeili, Mehdi, Nader Jalili and Mohammad Durali (2007). Dynamic modeling and performance evaluation of a vibrating beam microgyroscope under general support motion. *Journal of Sound and Vibration* **301**(1), 146–164.

Gallacher, Barry J., John Hedley, James S. Burdess, Alun James Harris, Alexandria Rickard and David O. King (2005). Electrostatic correction of structural imperfections present in a microring gyroscope. *Journal of Microelectromechanical Systems* **14**(2), 221–234.

Leland, Robert P. (2003). Adaptive mode tuning for vibrational gyroscopes. *IEEE Transactions on control systems technology* **11**(2), 242–247.

Oropeza-Ramos, Laura A. (2007). Investigations on novel platforms of micro electro mechanical inertial sensors: Analysis, construction and experimentation. *Phd Thesis, University of California, Santa Barbara*.

Oropeza-Ramos, Laura A. and Kimberly L. Turner (2005). Parametric resonance amplification in a memgyroscope. *Sensors, 2005 IEEE* pp. 660–663.

Oropeza-Ramos, Laura A., Christopher B. Burgner, Craig Olroyd and Kimberly L. Turner (2007). Characterization of a novel memgyroscope actuated by parametric resonance. *ASME IDETC Conference*.

Park, S. and R. Horowitz (2003). Adaptive control for the conventional mode of operation of mems gyroscopes. *Journal of Microelectromechanical Systems* **12**, 101–108.

Rhoads, J. F., S. W. Shaw, K. L. Turner and R. Baskaran (2005). Tunable micromechanical filters that exploit parametric resonance. *Journal of Vibration and Acoustics*.

Shkel, A., R. T. Howe and R. Horowitz (1999). Modeling and simulation of micromachined gyroscopes in the presence of imperfections. *Int. Conf. On Modelling and Simulation of Microsystems*.

Turner, K. (1999). Applications and analysis of parametric resonance in microelectromechanical systems. *Phd thesis, Cornell University*.

Turner, Kimberly L., Scott A. Miller, Peter G. Hartwell,

Noel C. MacDonald, Steven H. Strogatz and Scott G. Adams (1998). Five parametric resonances in a microelectromechanical system. *Nature* **396**, 149–152.

Wang, Frank, Larry Hobbs and Marc Smith (2006). A silicon gyroscope with electronic frequency tuning. *Proceedings of IMECE2006*.

Yazdi, Navid, Farrokh Ayazi and Khalil Najafi (1998). Micromachined inertial sensors. *Proceedings of the IEEE* **86**(8), 1640–1659.

Zaman, Mohammad, Ajit Sharma, Babak Amini and Farrokh Ayazi (2004). Towards inertial grade vibratory microgyros: A high-q in-plane silicon-on-insulator tuning fork device. *Solid-State Sensor, Actuator and Microsystems Workshop. Hilton Head, South Carolina*.